The Thesis Committee for Valeriia Sobolevskaia
Certifies that this is the approved version of the following Thesis:

Rock physics calibration of sandstone-shale laminated systems via petrophysical inversion of acoustic logs

APPROVED BY
SUPERVISING COMMITTEE:

Carlos Torres-Verdín, Supervisor

Kamy Sepehrnoori

Rock physics calibration of sandstone-shale laminated systems via petrophysical inversion of acoustic logs

BY

Valeriia Sobolevskaia

Thesis

Presented to the Faculty of the Graduate School of

The University of Texas at Austin

in Partial Fulfillment

of the Requirements

for the Degree of

Master of Science in Engineering

The University of Texas at Austin

August 2020

Dedication

To my family, for sharing the joy of life, inspiring bold decisions, supporting through hardships and pushing me when I am ready to give up. Thank you for always being there for me. I will love you forever regardless space and time distance between us: from Texas to Russia, Sweden, Azerbaijan and back to the US. It was quite a journey and I would not be there without you. Thank you.

Acknowledgements

I would like to thank my supervisor Dr. Torres-Verdín, my reviewer Dr. Kamy Sepehrnoori and all PGE faculty members that I worked with during my two years in UT Austin. It was a unique experience. I am also grateful to my teammates for sharing their time, knowledge and emotions with me. A special word of gratitude goes to Tianqi Deng for his unselfish help, collaboration, patience and insightful technical conversations. I also appreciate all technical help from Joaquín Ambía and Roger Terzian and administrative and personal support from Rey Casanova. This project was funded by University of Texas at Austin's Research Consortium on Formation Evaluation, jointly sponsored by Aramco, Baker Hughes, BHP Billiton, BP, Chevron, CNOOC International, ConocoPhillips, ENI, Equinor ASA, ExxonMobil, INPEX, Lundin-Norway, Occidental, Oil Search Alaska, Petrobras, Repsol, Schlumberger, Shell, Total, Wintershall-DEA and Woodside Petroleum Limited.

Last but not least, I am deeply grateful to my family for their unconditional support throughout the whole program. Thank you for pushing me and making me believe in myself.

Abstract

Rock physics calibration of sandstone-shale laminated systems via petrophysical inversion of acoustic logs

Valeriia Sobolevskaia, MSE

The University of Texas at Austin, 2020

Supervisor: Carlos Torres-Verdín

Interpretation of seismic amplitude inversion products into petrophysical properties requires proper calibration of the underlying rock physics model. Traditional petrophysical calibration workflows make use of well logs, mud logs, core data, and geological information. The calibration can also be established from the petrophysical inversion of borehole acoustic measurements, where the spatial resolution of the measurements is the highest possible. However, well logs are often adversely impacted by noise, borehole environmental effects, and instrument-acquisition averaging across thinly laminated rocks. We develop a new inversion-based procedure to estimate petrophysical properties of rocks from borehole measurements of bulk density, and P- and S-wave slownesses with focus on the specific but common case of sandstone-shale laminated systems. The procedure is based on the separate inversion of borehole measurements prior to the estimation of layer-by-layer petrophysical properties. Applications to synthetic and field data verify that the separate inversion of density, and P- and S-wave acoustic slownesses improves the definition of rock-physics models compared to using well logs, especially across thin layers with contrasting properties. Maximum relative errors in inverted properties are 3% for bulk

density and 5% for slownesses, while the relative differences between well logs and true formation properties are up to 50% and 35% for bulk density and acoustic slownesses, respectively. Furthermore, separate inversion enables the quantification of uncertainty and reduces noise and deleterious borehole environmental effects commonly present in acoustic slowness logs. In noise-free cases, root-mean square errors for inverted porosity and volumetric concentration of shale after separate inversion are 2-19 times lower compared to results obtained from well logs, whereas the 95% confidence interval for fluid saturation decreases 1.5-2 times after separate inversion. However, additional data may be required to (a) overcome non-uniqueness in the presence of complex petrophysical-elastic models, (b) improve accuracy, and (c) reduce uncertainty of inversion results. The new inversion-based interpretation procedure is a practical alternative to quantify the limits of detection and resolution of seismic inversion products and can be used to improve the match between seismic amplitudes and well logs when estimating seismic wavelets.

Table of Contents

List of Tables

List of Figures

Chapter 1: Introduction

Reservoir characterization requires knowledge of lithological, storage, and flow properties such as rock classes, shale volume, porosity, fluid saturation and permeability, among other properties. Borehole measurements (i.e. well logs and core data) typically provide the most accurate assessment of these properties (Tiab and Donaldson, 2015). However, borehole measurements sense the reservoir locally and may not be representative of the global storage and flow properties between wells. To secure a better understating of the spatial distribution of reservoir properties, seismic amplitude data are often used as they typically exhibit the best spatial coverage among all measurement types. Seismic inversion provides estimates of elastic rock properties, which can then be transformed into petrophysical properties using a fit-for-purpose rock physics model (RPM). However, to obtain the best results possible, the RPM used in petrophysical analysis must be calibrated based on the available borehole measurements; this step is often referred to as RPM calibration. The first and most fundamental interpretation step, therefore, should be the inversion of borehole measurements into petrophysical and solid/fluid compositional properties. Inversion of seismic-related borehole measurements into petrophysical properties provides a reliable assessment of the rock properties that can be detected and quantified from seismic inversion products originating from either post- or pre-stack seismic amplitude data.

Seismic inversion estimates acoustic rock properties from seismic amplitudes. In the case of post-stack seismic amplitude data, seismic inversion delivers bandlimited P-wave impedance, while in the case of pre-stack seismic amplitude data it delivers P-wave velocity, S-wave velocity, and bulk density, or combinations of these three properties. Therefore, RPM calibration should rely solely on density and acoustic logs as the sources of information. These measurements are affected by adverse borehole environmental conditions (borehole rugosity, fractures, mudcake, etc.) and different types of noise (instrumental and electronic noise, processing errors, source

ringing, depth matching, and limitations of waveform processing, among others). Such effects may or may not be correlated between well logs, whereby standard data filtering procedures can give rise to unreliable results. Furthermore, homogeneous spatial properties are typically assumed in the RPM used for petrophysical interpretation. To obtain reliable estimates of fluid and petrophysical properties from well logs, the assumptions implicit in the RMP should be consistent with the volume of investigation of the measurements.

The accuracy of petrophysical inversion depends on the quality of the input data and the calibration of the underlying RPM, as well as on the uniqueness of rock acoustic responses. In thinly laminated rocks, acoustic logs can be impaired by averaging effects. When thin layers are shouldered by layers with large property contrasts, acoustic logs often exhibit spatial smoothing effects. This condition takes place due to the influence of the instrument geometry because the vertical resolution of sonic tools is defined by the length of the receiver array (Tang *et al.*, 2004). The smoothing effect of acoustic logs reduces the property contrast between different rock types and can lead to inaccurate petrophysical results when not accounted for in the interpretations (Peyret *et al.*, 2006). A number of processing (Hsu and Chang, 1987; Zhang *et al.*, 2000) and inversion-based techniques (Sinha, 1997; Sinha *et al.*, 2006; Yang *et al.*, 2011) have been developed to improve the spatial resolution of acoustic logs for the estimation of rock properties. However, these techniques are sensitive to noise and often assume vertical homogeneity, which is not applicable in the presence of thin beds.

Skelt (2004) also addressed the problem of fluid substitution in sandstone-shale laminated systems. Commercial software packages often significantly overestimate compressional sonic slowness at high values of shale concentration. Consequently, effects due to presence of light fluids are modelled to be larger in shaly and less porous rocks than in clean and porous sandstone, in contrast to the established theory (Brie *et al.*, 1995) and observations from laboratory and field measurements. This abnormal behavior could also lead to significant inaccuracy in RPM calibration in thinly laminated sedimentary systems.

The estimation of petrophysical and solid/fluid compositional properties of rocks is typically performed using a gradient-based linear joint inversion algorithm (Quirein *et al.*, 1986; Gallardo and Meju, 2004) or stochastic inversion. The latter strategy enables the estimation of uncertainty of inverted properties either by (a) sampling possible conditions from a probability density function (Tarantola, 1987), (b) using a sequential Gaussian simulation approach (Haas and Dubrule, 1994), or (c) both (Moyen *et al.*, 2007). However, inversion results obtained with traditional inversion algorithms can be inaccurate in thinly laminated formations because of noise and averaging effects present in the borehole measurements used as input. Furthermore, RPM calibration is an essential step to establish appropriate mixing laws and is often not integrated into commercial software. An alternative two-step approach for estimating petrophysical properties from multiple borehole measurements was developed by Ijasan *et al.* (2013). This approach mitigates spatial averaging effects inherent to well logs by first detecting layer boundaries, then estimating layer-by-layer physical properties separately for each well log available. During this step, a spatial sensitivity function is "deconvolved" from the well logs which makes it possible to compare well logs acquired in wells logged with different tools or drilled with different bit sizes and muds (Huang *et al.*, 2015). The second step is to use the estimated layer-by-layer properties as collective input for petrophysical inversion, i.e., to estimate porosity and fluid/solid composition. Elastic properties and bulk density at this point are usually simulated with linear mixing laws (Deng *et al.*, 2019). To overcome some of the limitations of gradient-based methods, Yang and Torres-Verdín (2015) used Bayesian inversion with Markov chain Monte Carlo (MCMC) sampling to transform the inverted layer-by-layer properties into petrophysical properties. This approach improves uncertainty estimation and removes bias associated with the initial guess (Tarantola, 2005), and it was subsequently improved and adapted for various inversion problems associated with the quantitative interpretation of well logs acquired in vertical and high-angle wells (Huang *et al.*, 2015; Maalouf and Torres-Verdín, 2018b; Deng *et al.*, 2019).

We adopt a similar two-step approach to calibrate the RPM using acoustic and density logs acquired in thinly laminated formations. First, layer boundaries are detected from the available

well logs; next, the available well logs are separately inverted to obtain layer-by-layer physical properties with their corresponding uncertainty. Results obtained from the latter step and their uncertainties are then used as input for joint Bayesian inversion with random walk MCMC (RWMCMC) sampling to obtain layer-by-layer estimates of volumetric concentration of shale, porosity, and fluid saturation. We account for the effect of thin bed laminations on elastic properties using the Backus averaging, and perform fluid substitution only in sandstone laminae. Synthetic examples confirm that the separate inversion of well logs reduces noise and spatial averaging effects and further improves the resolution of layer-by-layer elastic properties. Inverted petrophysical properties are in good agreement with model properties even in the presence of biasing noise. The inversion-based interpretation workflow is reliable and enables the testing of multiple RPMs for calibration of model parameters faster than traditional techniques. However, it is found that additional *a-priori* constraints and calibration points are necessary to obtain reliable estimates of petrophysical and fluid properties in the case of spatially complex rocks where the RPM cannot be uniquely defined with the available measurements.

Chapter 2: Methodology

The proposed interpretation method consists of three main parts: (1) detection of layer boundaries from well logs, (2) separate inversion of acoustic logs to estimate layer-by-layer physical properties with their corresponding uncertainties, and (3) layer-by-layer joint inversion of density and elastic properties to estimate petrophysical and fluid properties. Appendices A and B provide details about the methods used for separate inversion of well logs and the estimation of layer petrophysical properties from inverted layer-by-layer bulk density and P- and S-wave slownesses, respectively. The general workflow steps are described in Figure 1 as follows: First, we define layer boundaries using a well log of choice; typically, gamma ray and density logs are the best candidates due to their relatively high resolution. We utilize the maximum variance method with a sliding window size adapted for each formation. Alternative methods such as maximum second-order difference, maximum magnitude, etc., can also be used for this purpose. Next, separate inversion of well logs (density and P- and S-slowness) is performed to obtain layer-by-layer bulk density, and P- and S-wave slownesses, together with their uncertainties. Density logs are simulated using the UTNuPro algorithm (University of Texas – Nuclear Properties, Goodyear *et al.* (2018)) and fast nuclear modeling methods (Mendoza *et al.*, 2010). To improve vertical resolution and reduce deleterious noise effects, axial sensitivity functions are used to simulate acoustic logs (Maalouf and Torres-Verdín, 2018b). For inversion, a likelihood function quantifies the mismatch between the measured well log and its numerical simulation and is subject to *a-priori* estimate of measurement uncertainty. The latter uncertainty is calculated based on the level of noise expected for a particular combination of tool type and borehole conditions. P- and S-wave acoustic logs are inverted jointly to comply with physical constrains, such as maintaining the P- to S-wave velocity ratio above a minimum physical value of $\sqrt{2}$.

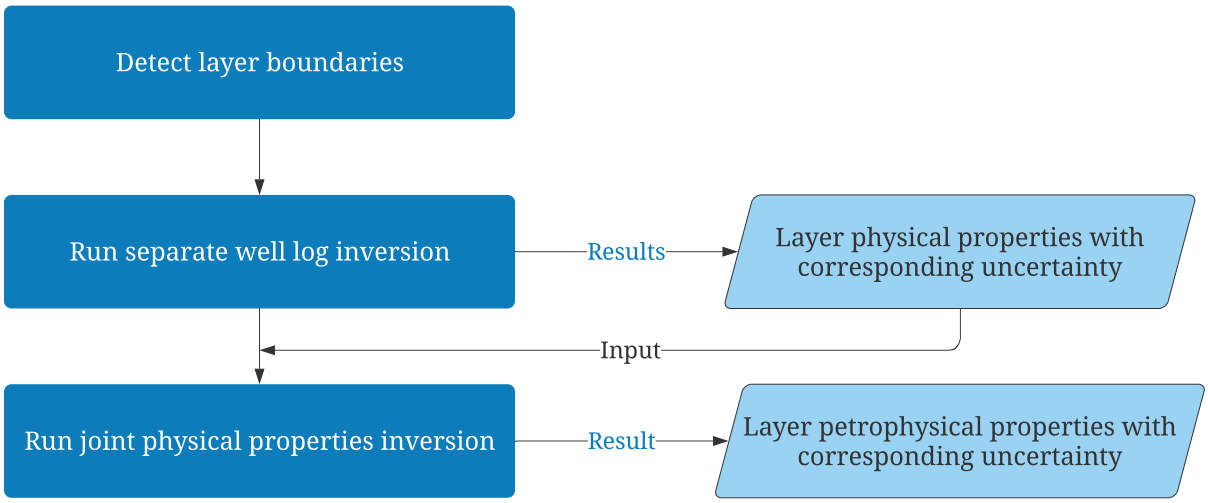

Figure 1. Workflow of the proposed inversion-based interpretation method for calibration of the rock-physics model.

Using the results obtained from the separate inversion, porosity and solid/fluid compositional properties are then estimated using joint Bayesian inversion with RWMCMC sampling. If additional data are available (e.g. core data or ancillary well logs), they can also be used as *a-priori* constraints. This step is crucial for the regularization of the solution for cases when the problem is underdetermined, i.e. when the number of input data is smaller than the number of inverted properties. *A-priori* information also helps to choose a relevant RPM and reduces uncertainty in its parameters. In sandstone-shale laminated rocks with multiple fluids, fluid substitution is only performed in the sandstone laminae. We then upscale the estimated physical properties using the Backus averaging and assuming vertically transverse isotropy (VTI).

Forward modeling of physical properties using the RPM can be time consuming. Therefore, we approximate this calculation using a surrogate model. To build the surrogate model, first we generate a database of petrophysical properties regularly sampled from the expected property ranges. Thereafter, using the RPM, we calculate a grid of physical properties corresponding to the database. During the inversion, values in between grid points are interpolated using a radial basis function (RBF) of choice. Also, if grid values closely match the current layer physical properties (less than 5% normalized difference), then the corresponding petrophysical

properties from the database are tested during the first steps of the joint inversion. This strategy allows one to find the most accurate initial guess without the risk of being trapped in a local minimum during the petrophysical inversion. Appendix B provides more details about the combined use of the sampling grid and the RBF included in the interpretation workflow.

It is crucial to note here that one of the most important steps is the preliminary quality control of the input data. Even though separate inversion takes into account the presence of noise and spatial averaging effects of well logs, if the input logs are misaligned in depth the results will be unreliable. Also, to ensure proper estimation of physical properties and their uncertainty, the input data should be analyzed to estimate the background noise level, which requires specific knowledge of tool properties, such as length of the receiver array, borehole diameter, centralization, and data processing.

Because the final goal of the inversion workflow is to improve the interpretation of seismic inversion products into petrophysical properties, the workflow can be readily adapted for analysis of alternative input properties such as acoustic impedances, elastic constants, or any combinations of their product. Similarly, depending on the complexity of the model and preferred output parameters, inversion products can be adapted too (e.g., inversion for shale content vs. inversion for mineral composition). Additionally, the RPM of choice may or may not be representative of a particular data set (Mavko *et al.*, 2020). Therefore, the workflow described above must be iterated to find the best RPM and calibrate its relevant parameters.

Chapter 3: Data Overview

Several examples are provided below to verify the applicability and limitations of the proposed RPM calibration workflow. The first two models are synthetic data sets based on an actual well penetrating a fluvial deltaic system. They include thinly laminated clastic formations with layer thickness ranging from 3.5 to 25 ft. Laminae in each layer consist of either sandstone or shale. Shale properties are assumed to be constant while sandstone porosity varies from lamina to lamina. Total layer porosity is a function of (a) pure sandstone porosity, (b) pure shale porosity, and (c) volumetric concentration of shale. Pores in sandstone laminae can be occupied by either water or methane, while shale is saturated with water only. Two non-communicating gas reservoirs are modeled with an underlying aquifer, where one of the reservoirs exhibits a gradual capillary transition to the aquifer and the remaining one a rapid capillary transition. However, the models differ in (a) mineralogical composition of shale and (b) porosity range of sandstone laminae. In the first model, pure shale consists of 30% illite, 15% quartz, and 55% kaolinite, and has 8% porosity, whereas sandstone laminae are 100% quartz with porosity varying from 15 to 25% (Figure 2). As shown in Figure 3 (top row), this combination of properties leads to pure shale being acoustically slower (and having lower acoustic impedance) than pure sandstone. In the second model, pure shale is comprised of 55% illite, 35% quartz, and 10% dolomite, and has the same as before 8% porosity, whereas sandstone laminae have the same composition of the previous model but are more porous (20 to 30%) (Figure 4). Hence, as shown in Figure 3 (bottom row), in this latter model pure shale is acoustically faster and denser than pure sandstone.

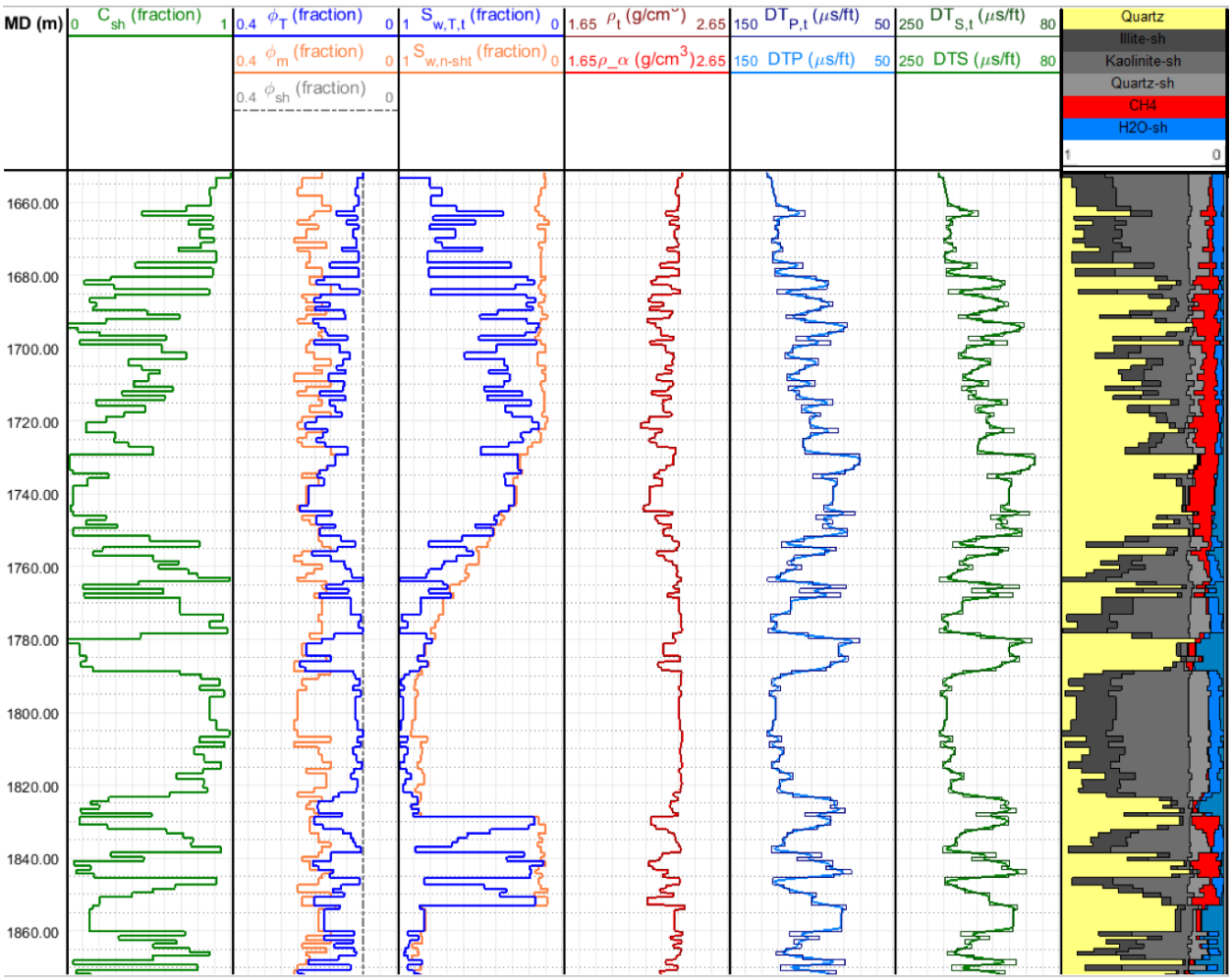

Figure 2. Synthetic Example No. 1. From left to right by track number: (1) Measured depth, MD, in m; (2) volumetric concentration of shale, C_{sh} (green); (3) shale porosity, ϕ_{sh} (gray), sandstone porosity, ϕ_m (orange), total porosity, ϕ_T (blue); (4) sandstone water saturation, $S_{w,n-shl}$ (orange), total water saturation, $S_{w,T,t}$ (blue); (5) modelled layer bulk density, ρ_t (dark red), and simulated density log, ρ_α (red); (6) modelled layer effective vertical P-wave slowness, $DT_{P,t}$ (dark blue), and simulated P-wave sonic log, DTP (blue); (7) modelled layer effective vertical S-wave slowness, $DT_{S,t}$ (dark green), and simulated S-wave sonic log, DTS (blue); (8) total mineral and fluid composition.

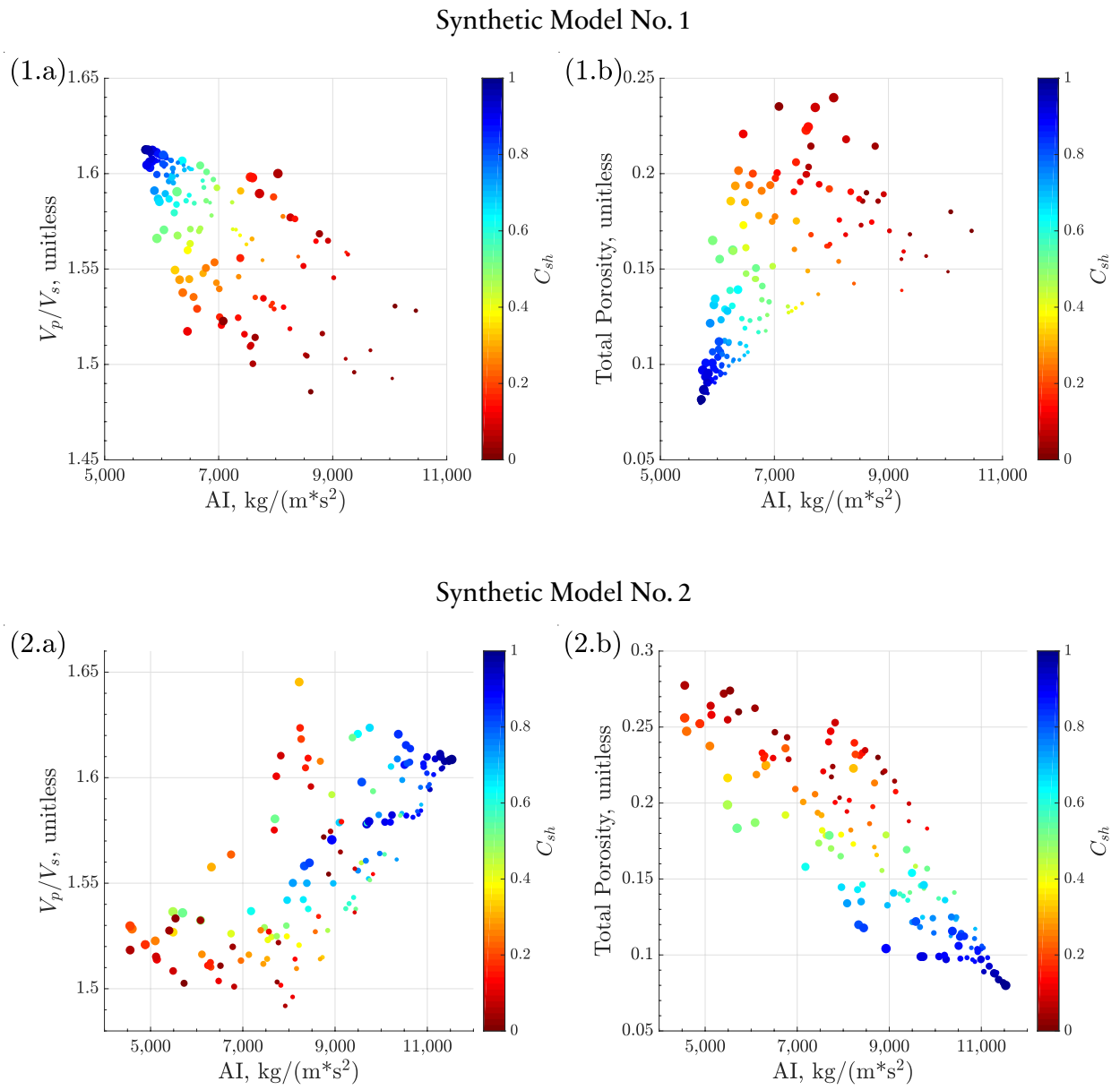

Figure 3. Cross-plots of acoustic properties for Synthetic Example No. 1 (top row) and Synthetic Example No. 2 (bottom row). (a) Acoustic impedance vs. velocity ratio colored by volumetric concentration of shale and point size based on matrix porosity. (b) Acoustic impedance vs. total porosity colored by volumetric concentration of shale and point size based on matrix porosity/

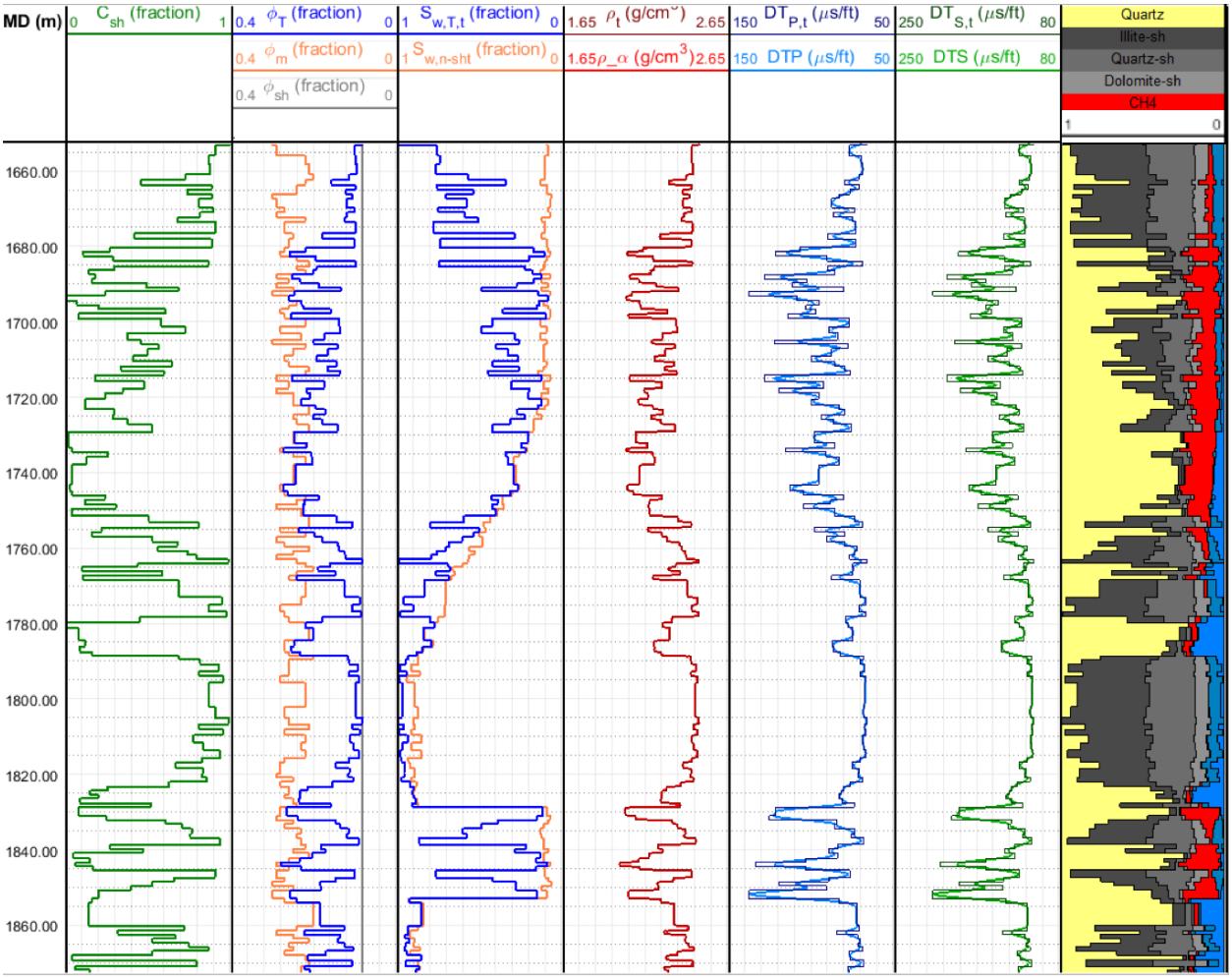

Figure 4. Synthetic Example No. 2. From left to right by track number: (1) Measured depth, MD, in m; (2) volumetric concentration of shale, C_{sh} (green); (3) shale porosity, ϕ_{sh} (gray), sandstone porosity, ϕ_m (orange), total porosity, ϕ_T (blue); (4) sandstone water saturation, $S_{w,n-shl}$ (orange), total water saturation, $S_{w,T,t}$ (blue); (5) modelled layer bulk density, ρ_t (dark red), and simulated density log, ρ_α (red); (6) modelled layer effective vertical P-wave slowness, $DT_{P,t}$ (dark blue), and simulated P-wave sonic log, DTP (blue); (7) modelled layer effective vertical S-wave slowness, $DT_{S,t}$ (dark green), and simulated S-wave sonic log, DTS (blue); (8) total mineralogical and fluid composition.

Physical layer properties were obtained using the self-consistent approximation theory (Mavko *et al.*, 2020) with spherical inclusions of quartz and penny crack inclusions of clay minerals (aspect ratio equal to 0.05). Borehole logs were numerically simulated assuming a generic LWD sonic tool with a receiver array length of 8 ft. Simulated well logs were contaminated with noise to mimic measurements errors. The generated noise had a power-law distribution with

median value of 7% for acoustic logs, and a normal distribution with zero mean and 0.015 g/cm^3 standard deviation for density logs. To reproduce the influence of borehole washouts on well logs, severe spikes in acoustic logs were correlated with density spikes. Both models were tested with and without presence of noise.

We describe two field examples of application. The first data set originates from a fluvial deltaic reservoir, where the well is vertical and was drilled with water-based mud. The reservoir consists of thinly laminated sandstone-shale formations with layer thickness ranging from 1.5 to 13 ft. There are two hydrocarbon-filled zones which are separated by a wet zone. Core measurements are available at several depths. Therefore, petrophysical calculations (total porosity and water saturation) were calibrated based on core data, while volumetric concentration of shale was calculated based on the gamma-ray log. Shear-wave data were not acquired in this well. However, as shown in Figure 5, clean sandstone and pure shale are well differentiated in P-wave slowness vs. bulk density cross-plots.

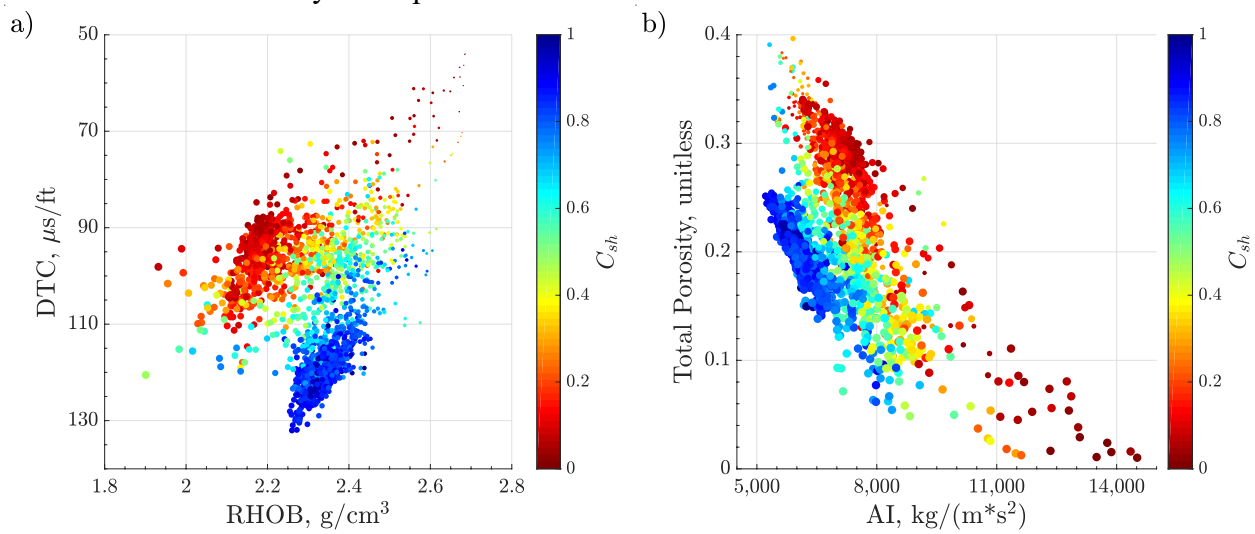

Figure 5. Cross-plot of acoustic properties for Field Example No. 1. (a) Bulk density vs. P-wave slowness colored by volumetric concentration of shale and point size based on total porosity. (b) Acoustic impedance vs. total porosity colored by volumetric concentration of shale and point size based on total water saturation.

The second field example describes a Middle Miocene turbidite system in the deepwater Gulf of Mexico. The well was drilled with water-based mud and penetrated a water-filled, thinly

laminated sandstone-shale formation with layers thickness varying from 1 to 15 ft. Core data were not available for this well. Therefore, volumetric concentration of shale was calculated from three different measurements, i.e. gamma-ray log, neutron-density logs, and R_t scanner (tri-axial induction resistivity measurements, mark of Schlumberger) logs. The latter logs are assumed to be the most accurate due to their deeper depth of investigation. Hence, shale concentration obtained using triaxial resistivity measurements was calibrated to shale concentration derived from the gamma-ray log and used for comparison. In both field examples, we detected layer boundaries using the bulk density log; however, layers thinner that 3.5 ft were grouped together due to the limitations of LWD acoustic tool resolution. Shear and bulk moduli for pure shale and pure sandstone (wet elastic moduli) were calculated in the "cleanest" depth sections adjacent to the zone of interest. The caliper log was also used in the analysis to quantify uncertainty due to rapid variations of borehole diameter (due to washouts).

Chapter 4: Results and Observations

The number of iterations in the MCMC inversion for synthetic and field examples was set to 10,000, with up to 40,000 additional iterations in layers with combined data mismatch above 1%. In all the tested conditions, it was found that the separate inversion of density, and P- and S-wave acoustic slownesses improved the definition of rock-physics models used to relate elastic and petrophysical properties, especially across thin layers with contrasting properties. In both synthetic cases, when tested without noise all layer-by-layer true properties fell within the 95% confidence interval of the inverted property (Figure 6). However, uncertainty in estimated slownesses increased with decreasing layer thickness. Note that in thin layers with high contrasting properties with respect to those of adjacent layers, the difference between true layer property and the midpoint sonic log value was up to 20%. Therefore, it was found that using well logs directly for petrophysical inversion gave rise to significant errors in the estimated properties.

In the presence of synthetic measurement noise, separate inversion allows one to mitigate the impact of noise in petrophysical calculations. With median 7% of noise in acoustic logs (power law distribution) and zero-mean, 0.015 g/cm^3 standard deviation (normal distribution) noise in the density log, separate inversion yielded accurate physical properties in all layers. The maximum relative error in the inverted properties was only 3% in bulk density and 5% in acoustic logs, corresponding to the mimicked washout zones while simulated noise-contaminated logs exhibited up to 50% and 35% relative error in density and acoustic logs, respectively (Figure 7). However, it should be noted that the uncertainty in the estimated property increases significantly due to borehole washouts, whose effect is modelled with relatively high noise levels. Well logs simulated from the inverted properties accurately reproduce noise-free logs. They are, therefore, recommended to be used in place of the original logs for the construction of synthetic seismograms and estimation of seismic wavelets (Maalouf and Torres-Verdín, 2018b).

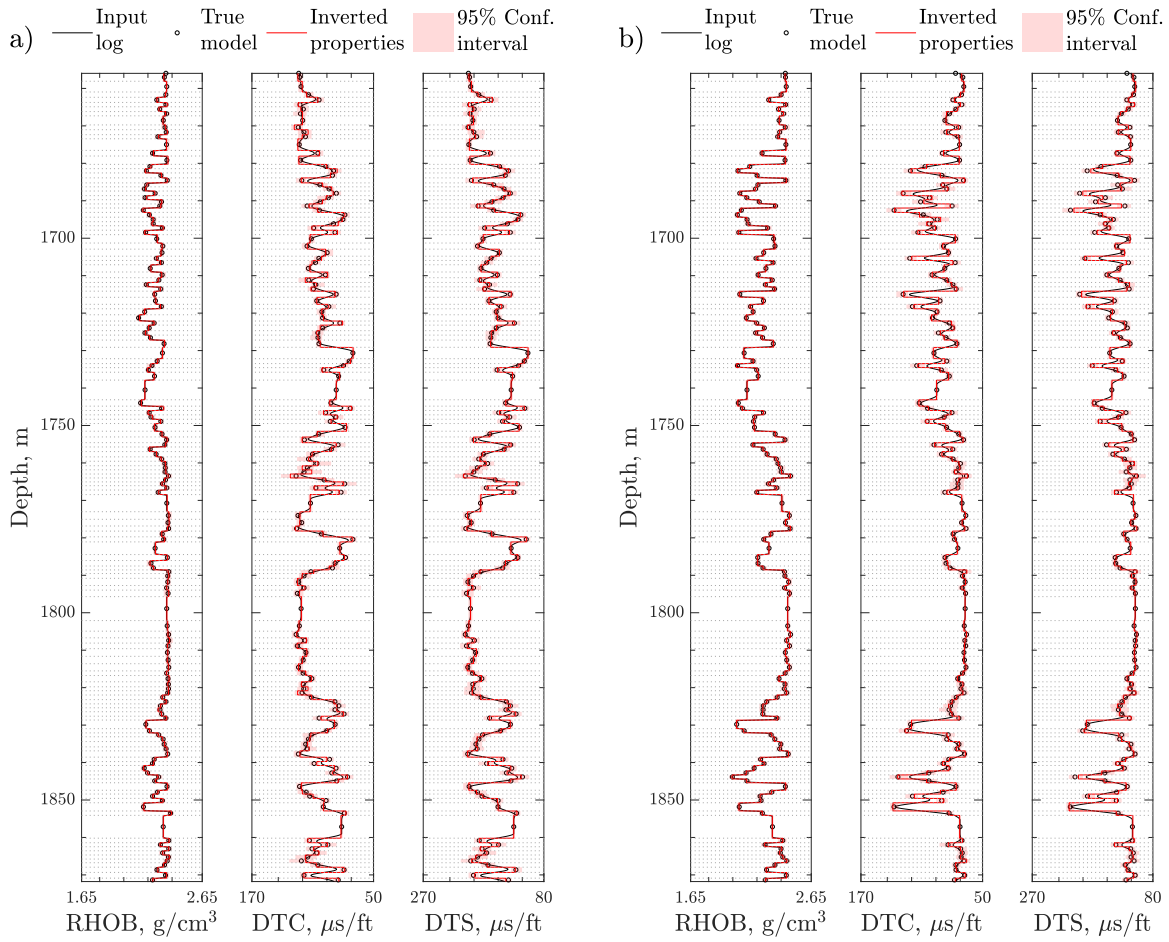

Figure 6. Separate inversion results for noise-free cases for Synthetic Model No. 1 (a) and Synthetic model No. 2 (b): input logs (black line), true model property (black circle), inverted layer property (red) with corresponding 95% confidence interval (pink). Logs or properties by track number: (1) bulk density, RHOB, g/cm^3, (2) P-wave slowness, DTC, μs/ft, (3) S-wave slowness, DTS, μs/ft.

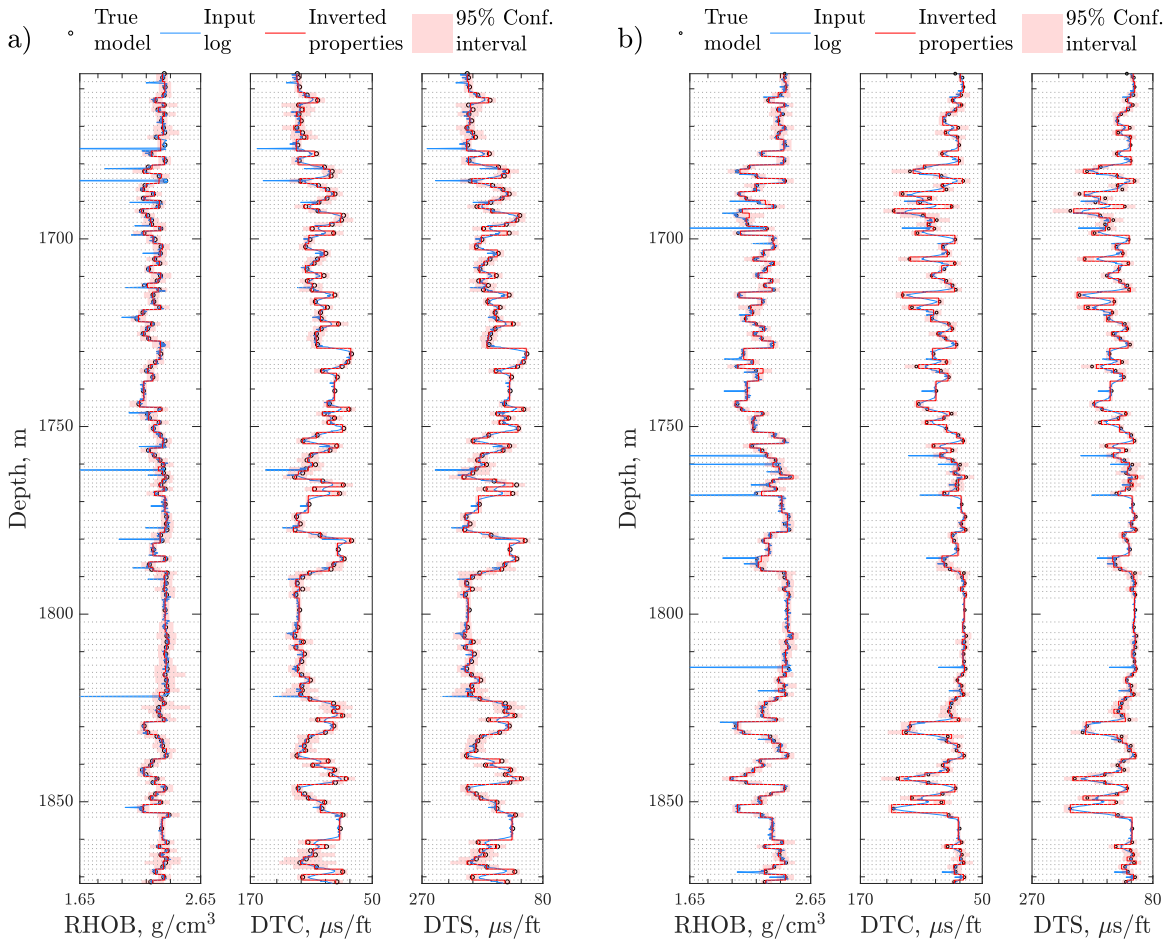

Figure 7. Separate inversion results for cases with added noise for Synthetic Model No.1 (a) and Synthetic Model No. 2 (b): input logs (blue line), true model property (black circle), inverted layer property (red) with corresponding 95% confidence interval (pink). Logs or properties by track number: (1) bulk density, RHOB, g/cm^3, (2) P-wave slowness, DTC, μs/ft, (3) S-wave slowness, DTS, μs/ft.

The blocky logs obtained with the separate inversion of density, and P- and S-wave slowness logs, in comparison to the actual well logs (midpoint values) improve the estimation of volumetric concentration of shale and porosity in shale-sandstone laminated systems. This effect is most prominent across thin layers with contrasting properties. With an appropriate RPM, when using the blocky logs (i.e., inverted layer-by-layer properties) in Synthetic Model No. 1 (where sandstones are faster than shales), the root-mean-square errors (RMSE) for volumetric concentration of shale, porosity and fluid saturation were 0.02, 0.01 and 0.15, respectively (Figure 8). Without preliminary separate inversion, RMSE values increase to 0.07, 0.02, and 0.21,

respectively (Figure 9). A similar trend was observed in Synthetic Model No. 2, where pure sandstone is slower than shale. Table 1 summarizes the RMSE values for all inverted petrophysical properties in different tested conditions and models. In all the examined cases, the accuracy of estimated fluid saturation is the lowest. This behavior occurs because of insufficient property contrast between water- and hydrocarbon-filled sandstone and uncertainty in layer physical properties. Inversion experiments showed that if uncertainty is set to an unrealistically low value in noise-free cases, then the RMSE in fluid saturation decreases to 0.01. However, in most cases this assumption is not valid, therefore fluid saturation can only be accurately estimated in highly porous clean sandstones.

RMSE FOR: / **CONDITION:**	**SHALE VOLUME**	**TOTAL POROSITY**	**WATER SATURATION**
SYNTHETIC NO. 1 (AFTER SEPARATE INVERSION)	0.02	0.01	0.15
SYNTHETIC NO. 1 (WITH MIDPOINT LOG VALUES)	0.07	0.02	0.21
SYNTHETIC NO. 1 (WITH NOISE AFTER SEPARATE INVERSION)	0.06	0.015	0.19
SYNTHETIC NO. 2 (AFTER SEPARATE INVERSION)	0.05	0.01	0.10
SYNTHETIC NO. 2 (WITH MIDPOINT LOG VALUES)	0.11	0.19	0.18
SYNTHETIC NO. 2 (WITH NOISE AND SEPARATE INVERSION)	0.12	0.02	0.19

Table 1. Summary of root-mean-square errors (RMSE) in the estimated petrophysical properties from jointly inverted density and P- and S-wave slownesses for the synthetic examples described in this paper.

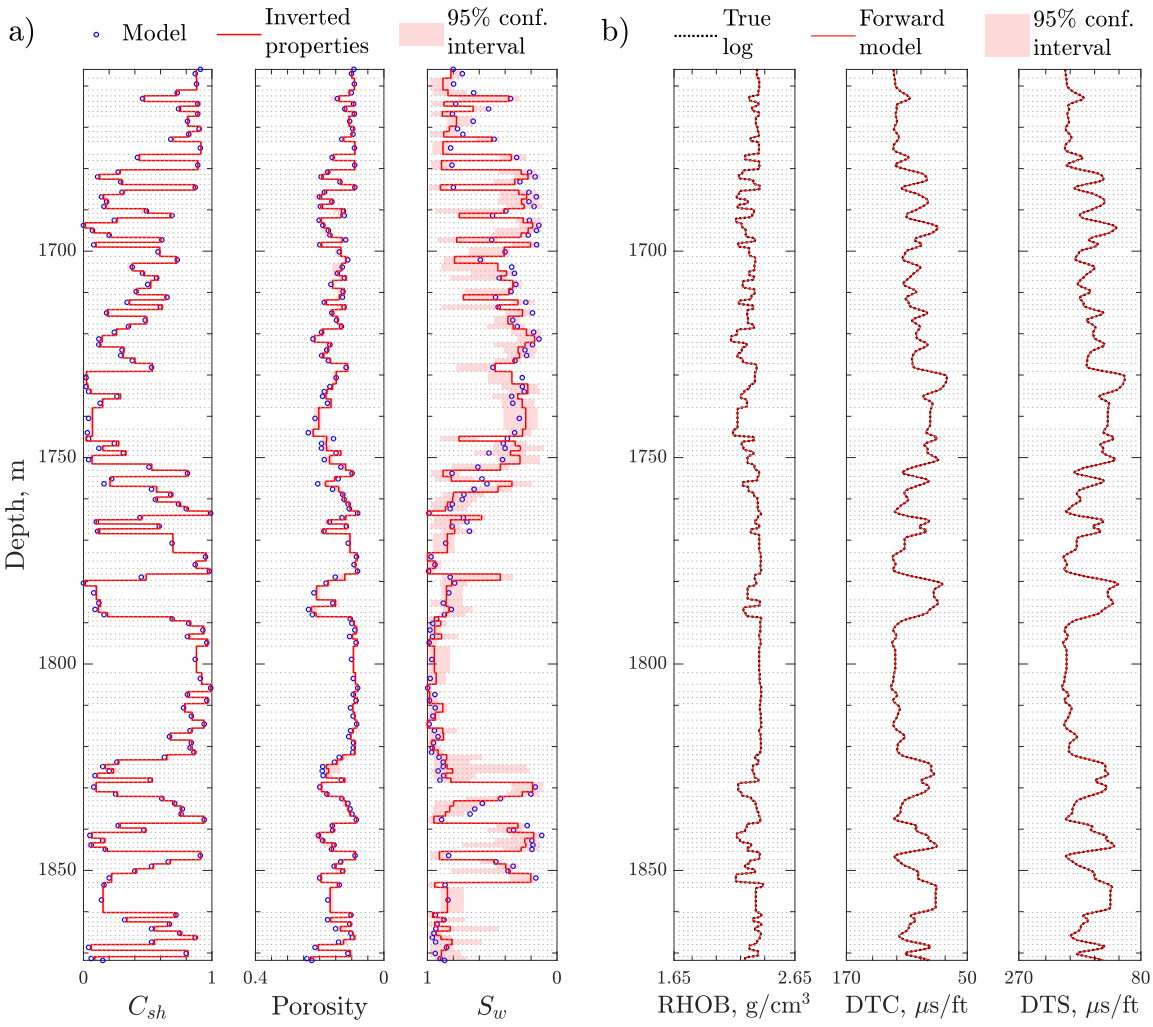

Figure 8. Synthetic Model No. 1. Joint inversion results when separate inversion results are used as an input. a) Inverted petrophysical properties (red) with 95% confidence interval (pink) and true model property (blue circles). b) Forward modelled logs (red) using joint inversion results with 95% confidence interval (pink) and original logs (black). Logs or properties by track number: (a) (1) volumetric concentration of shale C_{sh}, unitless, (2) total porosity, unitless, (3) total water saturation, S_w, unitless; (b) (1) bulk density, RHOB, g/cm^3, (2) P-wave slowness, DTC, μs/ft, (3) S-wave slowness, DTS, μs/ft.

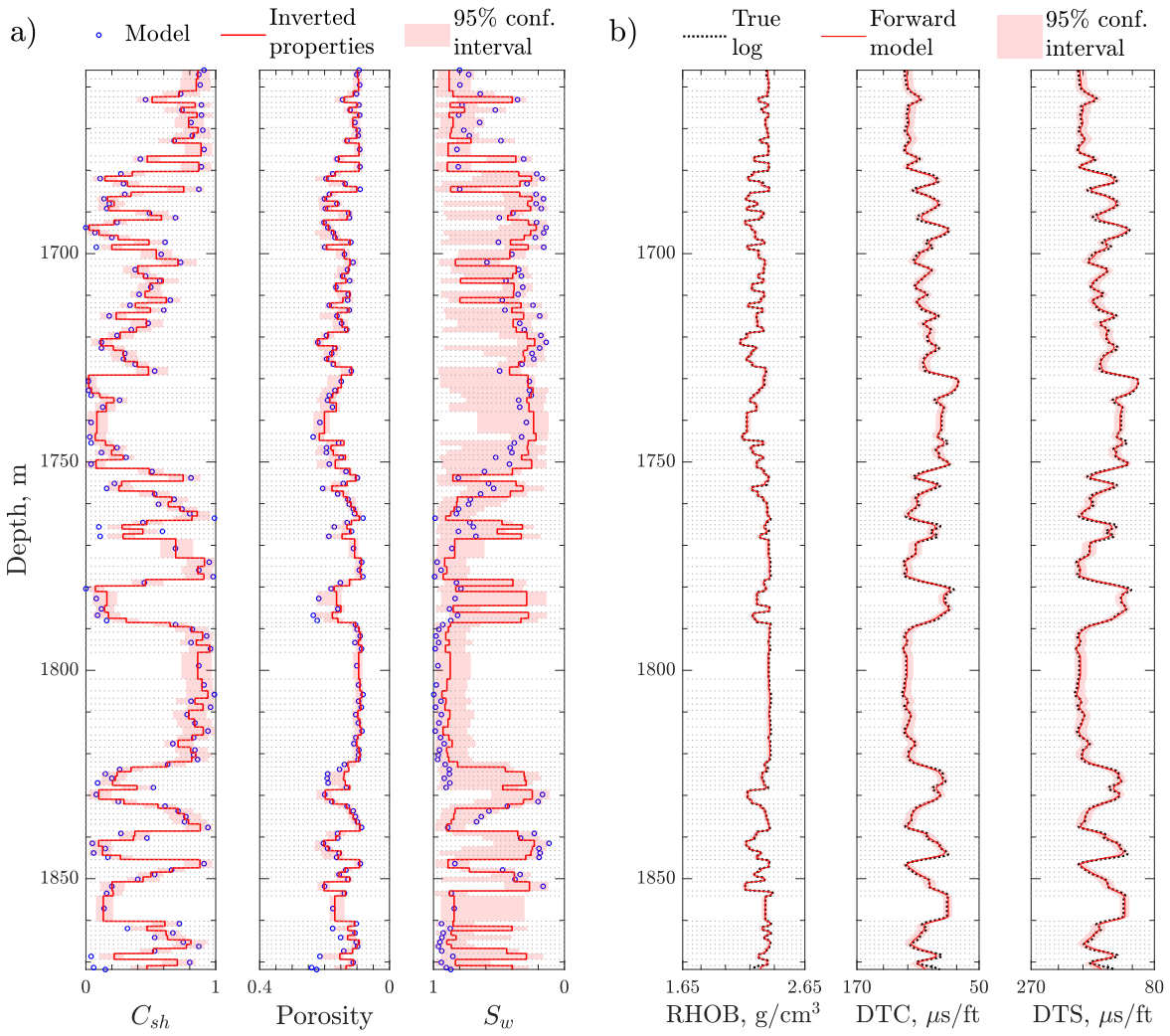

Figure 9. Synthetic Model No. 1. Inversion results without preliminary separate inversion (midpoint log value used as an input). a) Inverted petrophysical properties (red) with 95% confidence interval (pink) and true model property (blue circles). b) Forward modelled logs (red) using joint inversion results with 95% confidence interval (pink) and original logs (black). Logs or properties by track number: (a) (1) volumetric concentration of shale C_{sh}, unitless, (2) total porosity, unitless, (3) total water saturation, S_w, unitless; (b) (1) bulk density, RHOB, g/cm^3, (2) P-wave slowness, DTC, μs/ft, (3) S-wave slowness DTS, μs/ft.

Another benefit of performing preliminary separate inversion of physical properties is uncertainty estimation. When borehole measurements are used directly as input for joint inversion, uncertainty is typically estimated either as percentage of a log value or as a constant value along the well. However, uncertainty across thin layers should be significantly higher due to the limitations of tool resolution. Separate inversion allows one to quantify uncertainty of the

estimated layer-by-layer properties, which can be used thereafter to calculate uncertainty in petrophysical inversion. For Synthetic Model No. 1, the average width of the 95% confidence interval for fluid saturation when blocky logs (i.e., layer-by-layer inverted properties) are used is 36% (Figure 8). Without separate inversion, the average width of the 95% confidence interval is 50%, and it can be as high as 78% (Figure 9).

The key difference between the two presented synthetic models is that in Synthetic Model No. 1 pure shale is softer (lower acoustic impedance) than sandstone while in Synthetic Model No. 2 pure shale is harder (higher acoustic impedance) than pure sandstone (Figure 3). Our analysis indicates that petrophysical inversion results are more accurate when shale exhibits higher acoustic impedance (i.e., it is denser and/or acoustically faster) than water-filled sandstones. It is difficult to detect fluid in sandstones when pure (shale-free) sandstones are faster and/or denser than shales (higher acoustic impedance than pure shale). For noise-free cases, the RMSE values for volumetric concentration of shale and porosity were the same for both models. However, the RMSE for fluid saturations in the "fast sandstone" condition was 0.15, whereas in the "fast shale" model it was only 0.08 (Figure 8 and Figure 10).

Field examples confirm the importance of preliminary separate inversion in thinly laminated systems and highlight the limitations of the method. In the first field example, only bulk density and P-wave slowness logs were available for the interpretation. The minimum layer thickness was limited by the resolution of P-wave slowness log. However, the bulk density log has higher resolution than the P-wave sonic log. Hence, separate inversion in this well improves the definition of layer P-wave slowness (Figure 11a), while layer density values are intrinsically averaged so that the density value in the center of the layer is no longer accurate. To regularize the solution stemming from joint inversion, we estimated a prior distribution of compositional properties from petrophysical interpretation results obtained from well logs. As shown in Figure 11b, joint inversion results are in good agreement with petrophysical interpretation results. RMSE values for inverted volumetric concentration of shale, total porosity, and water saturation are 0.12, 0.04, and 0.20, respectively. Estimated water saturation has the lowest accuracy and the highest

uncertainty. These results are consistent with our observations from synthetic data sets. When sandstone exhibits high P-wave velocity, it is difficult to accurately estimate the corresponding fluid saturation. With decreasing values of volumetric concentration of shale, the accuracy of the estimated water saturation decreases and its uncertainty increases.

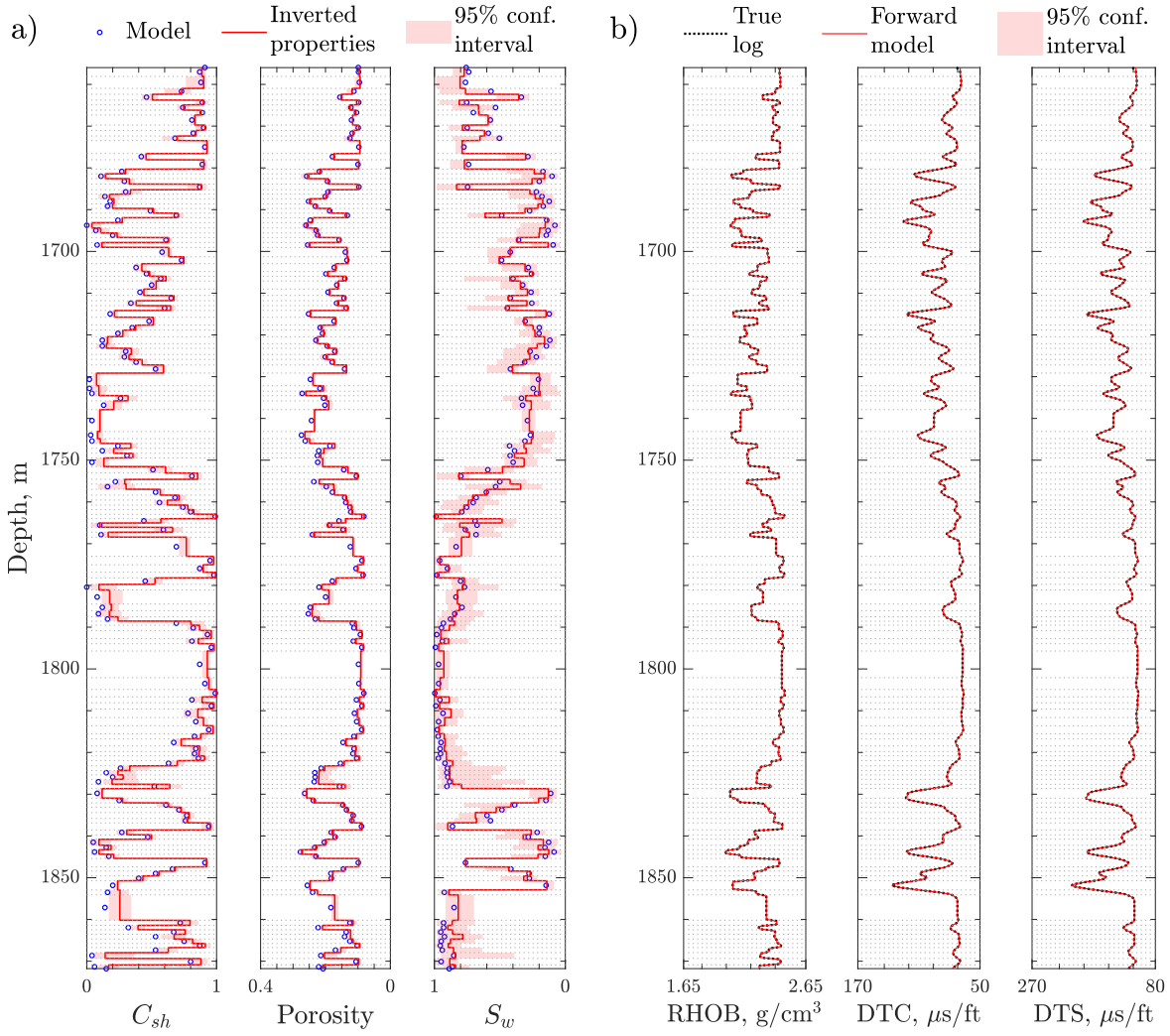

Figure 10. Synthetic Model No. 2. Joint inversion results when separate inversion results are used as an input. a) Inverted petrophysical properties (red) with 95% confidence interval (pink) and true model property (blue circles). b) Forward modelled logs (red) using joint inversion results with 95% confidence interval (pink) and original logs (black). Logs or properties by track number: (a) (1) volumetric concentration of shale C_{sh}, unitless, (2) total porosity, unitless, (3) total water saturation, S_w, unitless; (b) (1) bulk density, RHOB, g/cm^3, (2) P-wave slowness, DTC, μs/ft, (3) S-wave slowness, DTS, μs/ft.

.

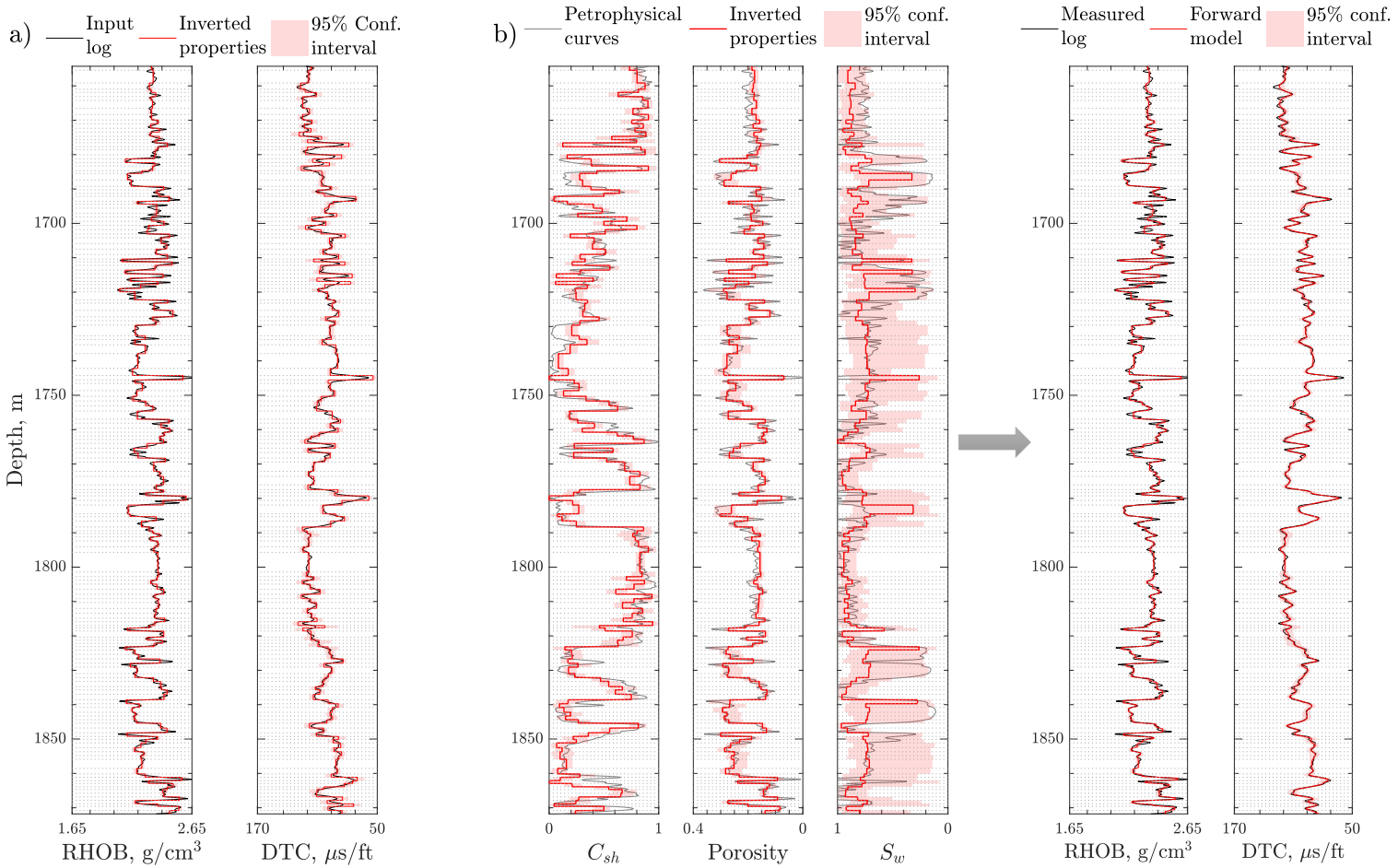

Figure 11. Field Example No.1. (a) Separate inversion results: input logs (black lines) and inverted properties (red lines) with 95% confidence interval (pink). Logs or properties by track number: (1) bulk density, RHOB, g/cm^3, (2) P-wave slowness, DTC, μs/ft. (b) Joint inversion results. (b) Petrophysical curves (grey lines) and inverted petrophysical properties (red) with 95% confidence interval (pink) and corresponding forward modelled logs (red) using joint inversion results with 95% confidence interval (pink) vs. measured logs (black lines). Logs or properties by track number: (1) volumetric concentration of shale, C_{sh}, unitless, (2) total porosity, unitless, (3) total water saturation, S_w, unitless, (4) bulk density, RHOB, g/cm^3, (5) P-wave slowness, DTC, μs/ft.

As shown in Figure 12a, in the second field example, the available borehole measurements are substantially affected by borehole washouts in the lower part of the interval of interest. Therefore, uncertainty in the inverted physical properties is higher in the borehole washout zone. The largest spikes were eliminated from the density log after performing the inversion. Acoustic logs were acquired with the Sonic Scanner tool (mark of Schlumberger), which has higher vertical resolution than a generic LWD acoustic tool. Additionally, most of the thin layers in this well are present in the washout zone. Therefore, there are only several layers where the inverted slowness differs from the corresponding center-point log value by more than 10%; inverted slownesses are also biased toward the mean value due to high uncertainty in the borehole washout zone.

There was no clear correlation between the well logs and the petrophysically estimated volumetric concentration of shale. Therefore, no additional prior constraints were used for joint inversion. Even though the model was calibrated in the "cleanest" sandstone and shale at the nearby depth interval, this well exhibits high variability in acoustic properties, which is most likely attributed to complex rock composition. Therefore, our calibration results might not be valid for all layers in the tested interval. The inverted volumetric concentration of shale follows a general trend of shale concentration estimated from Rt-Scanner measurements (Figure 12b), however, it does not agree well with the volumetric concentration of shale calculated with Rt-Scanner measurements; RMSE values are 0.17 and 0.37 when comparing the general trends and the fine scale, respectively. This behavior can be due to both unresolved layers by the acoustic tools and variability of rock properties not accounted for by our inversion process (i.e., varying shale or sandstone composition or varying pure-shale porosity). In this field example, well logs simulated from inverted properties do not accurately reproduce the original input logs. In comparison to the first field example, RMSE for simulated density and P-wave slowness logs are 2 and 3.5 times higher, respectively. This mismatch points at either a poorly calibrated model, RPM limitations, a more complex underlying rock model, or unreliable borehole measurements due to severe washouts. It follows that prerequisite information might not be adequate to describe the model given the complexity of the formation and borehole conditions. Therefore, the usage of additional

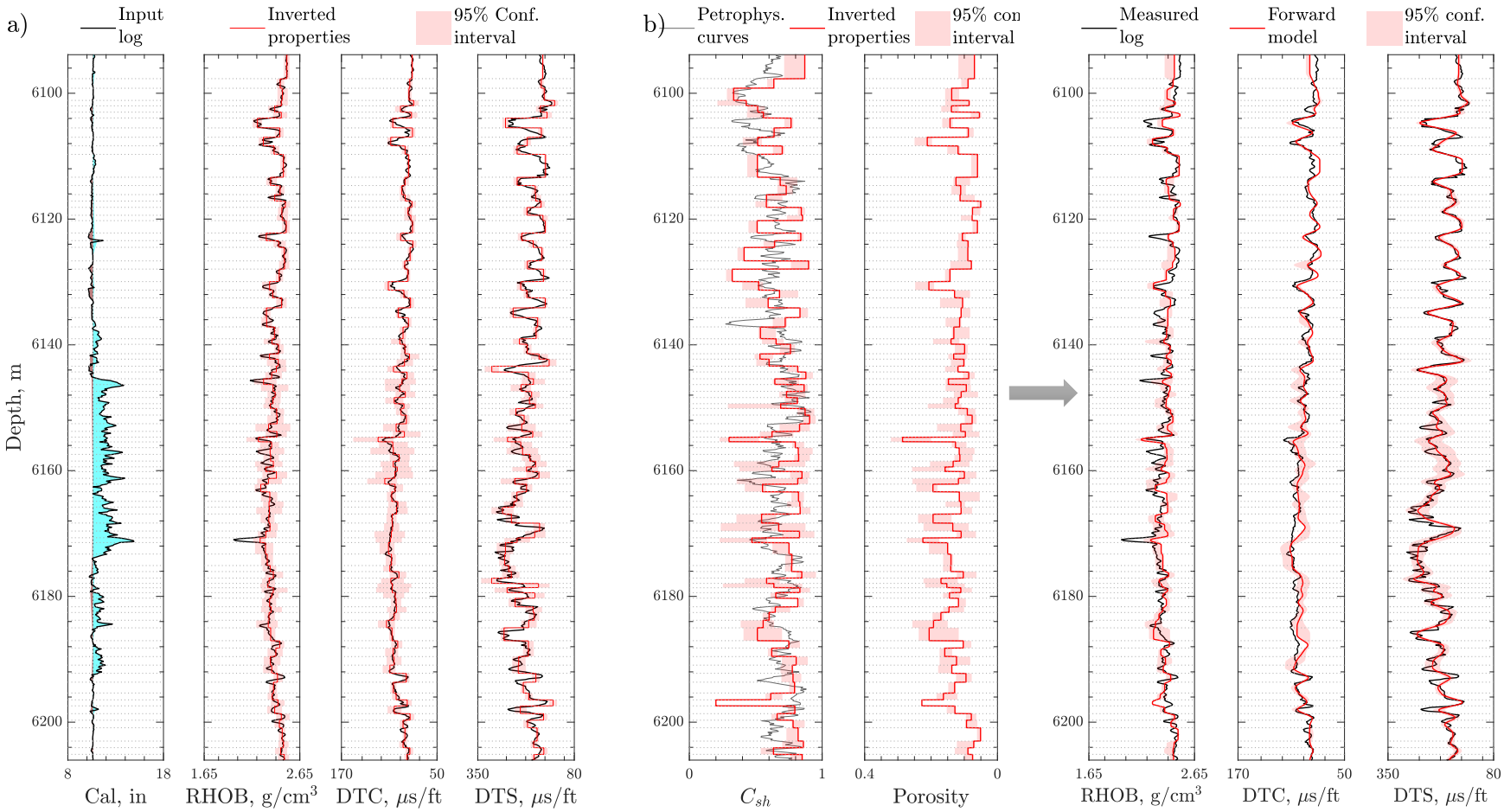

Figure 12. Field Example No.2. (a) Separate inversion results: input logs (black lines), washed out zones (cyan), and inverted properties (red lines) with 95% confidence interval (pink). Logs by track number: (1) caliper, Cal, in, (2) bulk density, RHOB, g/cm^3, (3) P-wave slowness, DTC, μs/ft, (4) S-wave slowness, DTS, μs/ft. (b) Joint inversion results: petrophysical curves (grey lines), inverted petrophysical properties (red) with 95% confidence interval (pink) and corresponding forward modelled logs (red) using joint inversion results with 95% confidence interval (pink) vs. measured logs (black lines). Logs or properties by track number: (1) volumetric concentration of shale, C_{sh}, unitless, (2) total porosity, unitless, (3) bulk density, RHOB, g/cm^3, (4) P-wave slowness, DTC, μs/ft, (5) S-wave slowness, DTS, μs/ft.

data or more reliable well logs would be beneficial for model calibration and could potentially improve the inversion results.

Chapter 5: Conclusions

The inversion-based interpretation method introduced in this paper robustly and efficiently estimates petrophysical properties from bulk density and acoustic logs. When noisy logs are used directly as input for joint inversion, noise deleteriously propagates to the inversion products and can render the corresponding interpretations unreliable. Through separate well-log inversion, our method reduces noise and spatial averaging effects commonly encountered across thinly laminated formations. The maximum relative error in the presence of noise is 3% for inverted density and 5% for inverted formation slownesses, while the relative error is up to 50% and 35% for bulk density and slownesses, respectively, when the calculations are performed without separate well-log inversion. Synthetic and field examples of application verified that well logs simulated from inverted properties closely match noise-free logs. Therefore, we recommend using simulated logs instead of original noise-contaminated well logs for well ties and wavelet estimation. Additionally, separate inversion enables the comparison of borehole measurements acquired in different wells with different instruments because it implicitly mitigates the influence of tool geometry and reduces borehole environmental effects (e.g., washouts). This attribute is important for management of fields where wells have been drilled at different times and logged by different service companies, or with different instruments.

Separate inversion also quantifies uncertainty in the estimation of properties due to tool resolution, layer thickness, well-log quality, and property contrast. Examples of application highlight the importance of this step in thinly laminated systems with highly contrasting layer properties. Averaged log values can differ from true layer properties by up to 20%, thereby introducing bias in the calibration of the RPM. In noise-free cases, RMSE values for inverted porosity and volumetric concentration of shale after separate inversion are 2-19 times lower in comparison to results obtained from traditionally used center-point log values. Additionally, the width of the 95% confidence interval for fluid saturation decreases 1.5-2 times after separate inversion. It was also found that the estimated volumetric concentration of shale and porosity are

typically more accurate than fluid saturation. On average, RMSE values for fluid saturation are 3-5 times higher than for other properties which is due to a lower contrast in physical properties. This behavior is especially challenging in cases where sandstone is acoustically faster than shale.

Another important advantage of the proposed inversion-based interpretation method for RPM calibration is its efficient computer performance: It enables testing of different RPMs, property ranges, and solid/fluid composition in minutes of CPU time to obtain accurate model calibrations before seismic inversion. The improvement in computation time is achieved through a reduced number of samples after separate inversion, implementation of RBFs, and an effective sampling algorithm. Without using RBFs, the computational time for a model of 100 layers increases by approximately 1,000 times, whereas without separate inversion it increases 3-10 times depending on layer thickness and log sampling rate. As a result, with the proposed workflow an interpreter can test a wider range of petrophysical parameters, leading to a more accurate RPM calibration. Our inversion-based interpretation method can also be easily adapted for different types of input logs and target properties, which makes it attractive for users of different commercial software and when working under various field conditions. The procedure can also be used to verify the potential of facies-based seismic inversion by testing whether the facies are acoustically distinguishable. This condition is important in many geological settings, for example, in reservoirs where low porosity cemented sandstones can be confused with shaly intervals.

Finally, it is important to emphasize that with increasing formation complexity the uncertainty of inversion results increases. To obtain reliable results, the model should be benchmarked against additional data sources, such as core data, or petrophysical estimations performed with well logs and validated with core laboratory measurements. In the presence of borehole washouts, extreme rock variability, and rock classes with similar elastic properties, it may be challenging to obtain reliable results without the use of additional constraints. Therefore, modelling assumptions and underlying uncertainty should always be calculated and delivered together with the estimated properties.

Appendices

APPENDIX A

METHOD USED FOR THE SEPARATE INVERSION OF WELL LOGS

Separate inversion of well logs is the first step in our workflow. It allows one to obtain layer-by-layer physical properties and their uncertainty from borehole measurements of bulk density, and P- and S-wave slownesses. These results are then jointly inverted to obtain petrophysical properties, such as volumetric concentration of shale (or mineralogical composition of rocks), porosity, and fluid saturations.

Grana and Della Rossa (2010) introduced the original Bayesian workflow for petrophysical inversion of elastic properties estimated from seismic inversion products. We adopt a similar approach in both steps of our workflow to obtain a posterior distribution, *P,* of a property of interest given the input data. For separate inversion, Bayes's theorem can be written as

$$P(\boldsymbol{d}|\boldsymbol{l}) \propto p(\boldsymbol{d})\, L(\boldsymbol{l}|\boldsymbol{d}), \tag{A-1}$$

where $\boldsymbol{d}$ is a layer physical property (bulk density or acoustic slowness), $\boldsymbol{l}$ is the input well logs (borehole measurement of density or slowness), p is *a-priori* distribution and L is a likelihood function. The likelihood function, L, depends of the misfit between the input well log, $\boldsymbol{l}$, and the numerically simulated log, $\boldsymbol{S}(\boldsymbol{d})$, using the proposed layer properties, $\boldsymbol{d}$, as well as the noise realization, $\boldsymbol{n}$, in each layer, and is given by

$$L(\boldsymbol{l}|\boldsymbol{d}) \propto \exp\left[-\frac{1}{2}[(\boldsymbol{S}(\boldsymbol{d})-\boldsymbol{l})^T\, \boldsymbol{N_n^{-1}}(\boldsymbol{S}(\boldsymbol{d})-\boldsymbol{l})]\right], \tag{A-2}$$

where $\boldsymbol{N_n}$ a covariance matrix, i.e., an identity matrix multiplied by the squared inverse of the noise level (its standard deviation) associated with well logs. It should be noted that in synthetic noise-free models or field examples with no environmental effects (stable borehole conditions), the level of noise is assumed to be constant in each layer and defined only by the tool type, i.e., 0.015 g/cm^3 for the density log and 7% for acoustic slowness logs (Grana, 2013). However, in the presence of severe washouts, borehole measurements can become unreliable because they sense the borehole fluid instead of the formation. In this case, we estimate the noise level separately for

each point based on the derivative of the caliper log with respect to depth. We assume that rapid variations in caliper measurements indicate washout zones. As a result, severe washouts are assigned higher uncertainty and corresponding layers have higher noise level (higher standard deviation). A similar approach is applied to the *a-priori* distribution. The mean of the prior distribution is equal to the mean log value at the interval of interest in all cases. Its standard deviation in noise-free cases is constant for all layers and corresponds to the average noise level typical for this type of measurement. However, in noisy cases, it is weighted by the noise level estimated from the caliper log. Such assignment of weights and uncertainty allows one to bias the separately inverted properties toward the *a-priori* distribution instead of a local log value in depth zones with prominent borehole washouts. As a result, underestimated values of density or formation velocity in washout zones are replaced with more accurate average values.

Because we focus our analysis on laminated formations, shoulder-bed effects also need to be addressed in acoustic-log inversion. To that end, we implement an approach introduced by Huang *et al.* (2015). With the assumption that the well is vertical and formation layers are horizontal, the approach uses frequency-domain one-dimensional (1D, axial) sensitivity functions to rapidly simulate acoustic logs and then estimates layer-by-layer slownesses by iteratively matching the input and simulated logs. The idea behind this approach is that sensitivity functions define a relationship between the medium property and its measurement, i.e., they quantify the perturbation of the measurement caused by the spatial perturbations of a medium property. Axial sensitivity functions depend on frequency, formation property, wave mode, and tool geometry. Hence, inversion "deconvolves" the sensitivity function from the measured log to mitigate the influence of adjacent layers, geometry of the receiver array, and noise and to estimate layer properties. This step is crucial in thinly laminated formations with high contrast of layer properties, especially if the receiver array is longer than the thickness of the layers involved. Not only does this approach sharpen the logs and decreases noise influence, but also allows to compare acoustic logs obtained by different tools. Refer to Huang *et al.* (2015) and Maalouf and Torres-Verdín (2018a) for detailed descriptions about the theoretical background and implementation of this

method. Density logs are inverted independently using similar nuclear spatial sensitivity functions (Mendoza *et al.*, 2010). Note also that P- and S-wave acoustic logs are inverted jointly to comply with the physical constraint of a minimum P- to S-velocity ratio of $\sqrt{2}$.

APPENDIX B

METHOD USED FOR THE JOINT INTERPRETATION OF LAYER-BY-LAYER PROPERTIES SEPARATELY INVERTED FROM WELL LOGS

The second step in the proposed interpretation workflow is the joint inversion of layer physical properties. Results obtained from the previous step, i.e., layer bulk density and P- and S-wave slowness, together with their corresponding probability distributions, are used as input. We implement joint Bayesian inversion with RWMCMC sampling to obtain layer-by-layer petrophysical properties together with their uncertainty and compare the corresponding forward simulated log with the original well logs.

Petrophysical properties are jointly inverted from the previously estimated layer-by-layer physical properties using Bayes's theorem, given by:

$$P(\boldsymbol{m}|\boldsymbol{d}) \propto p(\boldsymbol{m})\, L(\boldsymbol{d}|\boldsymbol{m}), \tag{B-1}$$

where $\boldsymbol{m}$ is a layer petrophysical property (porosity, volumetric concentration of shale, and mineral or fluid fraction), $\boldsymbol{d}$ is the input layer physical property (bulk density and P- and S-wave acoustic slownesses), p is *a priori* distribution and L is a likelihood function. In this case, the prior distribution is obtained from additional data when available (i.e. core data, standard petrophysical curves), while the likelihood function is given by

$$L(\boldsymbol{d}|\boldsymbol{m}) \propto \exp\left[-\tfrac{1}{2}[(\boldsymbol{G}(\boldsymbol{m}) - \boldsymbol{d})^T\, \boldsymbol{Q_n}^{-1}(\boldsymbol{G}(\boldsymbol{m}) - \boldsymbol{d})]\right], \tag{B-2}$$

where $\boldsymbol{G}$ is an effective medium model (EMM) of choice, $\boldsymbol{Q}$ is the uncertainty distribution that is assumed to be proportional to the posterior distribution of physical layer properties (obtained from separate inversion). Additional constraints can be also added to regularize the solution, which can be based on external information, petrophysical interpretations, or core measurements. Depending on the relationship between the properties, either Gaussian Mixture Models (assuming that the

underlying distribution is a mixture of Gaussian distributions) or a functional correlation can be used to define the additional constraints. A functional correlation should be preferred when there is a single trend in the data to avoid uneven uncertainty distributions. The initial number of iterations to sample the posterior distribution is defined by the complexity of the model and must be tested for each dataset individually. However, some layers may need more iterations to find an optimum value than others. Hence, after the defined number of iterations are completed, the relative difference between the input and simulated properties is calculated. Because each layer is inverted independently, additional iterations are added in the layers where the error exceeds the predefined threshold. This approach allows one to improve the accuracy of the inversion results without significant increase in computation time.

One of the most time-consuming steps at this stage is the forward simulation of physical properties for a given rock composition using EMM. To circumvent this problem, we approximate the EMM calculations using a pre-calculated grid of physical properties and a radial-basis function (RBF, Fasshauer (2007)) to interpolate values between the grid points. For best performance, the grid should cover all the expected ranges of properties and be uniform in physical property space because the RBFs are sensitive to the limiting boundaries. Therefore, all mineral (or rock class) and fluid components are first uniformly sampled within the allowed limits and then combined into a database. Only those combinations of rock components that honor material balance (i.e., the sum of their volume fractions is equal to one) are kept in the database. Next, the grid of physical properties corresponding to the petrophysical database is calculated using the EMM of choice. The assumptions of the selected EMM should be applicable to the particular rock types present in the data. For quality control, the grid is cross-plotted with well logs. If the three-dimensional (3D) EMM-simulated property grid covers the field data cloud, then the chosen RPM adequately describes the field data set. Otherwise, the RPM parameters should be iteratively calibrated until the properties overlap. To obtain the corresponding response surface, the grid is interpolated using a Gaussian RBF, ϕ, given by

$$\phi(R) = \exp -(\epsilon R)^2, \qquad (3)$$

where ϵ is a shape parameter (typically a small value close to 1) and R is Euclidian distance between the points. Alternative kernel functions to RBFs can also be used for this purpose, such as multi-quadratic, inverse quadratic, polyharmonic spline, etc. Another benefit of using RBFs is that the grid can be used to identify the range of best-matching input values before performing the inversion. These values can be used as initial guesses and/or initially tested values. As a result, the algorithm will converge faster without biasing the results. Such a technique is most efficient in formations where different rock classes exhibit markedly distinct properties from each other in acoustic space.

Two additional steps are performed when this workflow is applied to laminated formations. First, at each iteration, forward simulation is run twice to estimate pure-shale and pure-sandstone density, and P- and S-wave slownesses corresponding to the proposed petrophysical properties. Fluid substitution is only performed in sandstone lamina when multiple fluids are present. To calculate effective layer properties, we use the Backus averaging, which allows to calculate vertical and horizontal effective slownesses for P- and S-waves based on elastic constants (Mavko *et al.*, 2020). We assume that formations can be described by Vertical Transverse Isotropy (VTI). This assumption allows one to reduce the number of independent elastic constants that are required to describe each layer and simplifies the effective stiffness tensor components as follows:

$$\begin{bmatrix} A & B & F & 0 & 0 & 0 \\ B & A & F & 0 & 0 & 0 \\ F & F & C & 0 & 0 & 0 \\ 0 & 0 & 0 & D & 0 & 0 \\ 0 & 0 & 0 & 0 & D & 0 \\ 0 & 0 & 0 & 0 & 0 & M \end{bmatrix}, \text{ where } M = \frac{1}{2}(A - B), \text{ and} \tag{4}$$

$$A = \left\{4\rho V_s^2 \left(1 - \frac{V_s^2}{V_p^2}\right)\right\} + \left\{1 - 2\frac{V_s^2}{V_p^2}\right\}^2 \left\{\frac{1}{\rho V_p^2}\right\}^{-1} \tag{5}$$

$$B = \left\{2\rho V_s^2 \left(1 - \frac{2V_s^2}{V_p^2}\right)\right\} + \left\{1 - 2\frac{V_s^2}{V_p^2}\right\}^2 \left\{\frac{1}{\rho V_p^2}\right\}^{-1} \tag{6}$$

$$C = \left\{\frac{1}{\rho V_p^2}\right\}^{-1} \tag{7}$$

$$F = \left\{1 - 2\frac{V_s^2}{V_p^2}\right\}^2 \left\{\frac{1}{\rho V_p^2}\right\}^{-1} \tag{8}$$

$$D = \left\{\frac{1}{\rho V_s^2}\right\}^{-1} \tag{9}$$

$$A = \{\rho V_s^2\}, \quad (10)$$

where brackets $\{...\}$ symbolize an averaged value of the expression inside weighted by the proportion of each rock type (i.e., volumetric fraction of shale in our case). From these components, the effective slownesses are calculated as:

$$s_{P,hor} = \sqrt{\frac{\rho}{A}} \quad (11)$$

$$s_{P,vert} = \sqrt{\frac{\rho}{C}} \quad (12)$$

$$s_{SH,hor} = s_{SV,hor} = s_{SV,vert} = \sqrt{\frac{\rho}{M}} \quad (13)$$

$$s_{SH,vert} = s_{SV,hor} = s_{SV,vert} = \sqrt{\frac{\rho}{D}}, \quad (14)$$

where $s_{P,hor}$ and $s_{P,vert}$ are slownesses of a P-wave propagating in the horizontal and vertical direction, respectively, $s_{SH,hor}$ and $s_{SH,vert}$ are slowness of a horizontally polarized S-wave propagating in the horizontal and vertical direction, respectively, and $s_{SV,hor}$ and $s_{SV,vert}$ are slowness of a vertically polarized S-wave propagating in the horizontal and vertical direction, respectively. Values measured with borehole sonic tools correspond to vertically propagating waves, hence these are the values that are further used in the forward modelling to calculate the likelihood function.

List of symbols

Volumetric concentration of shale	C_{sh}
Layer physical property	$\boldsymbol{d}$
Effective vertical P-wave slowness	$DT_{P,t}$
Effective vertical S-wave slowness	$DT_{S,t}$
Effective Medium Model operator	$\boldsymbol{G}$
Well logs	$\boldsymbol{l}$
Likelihood function	L
Layer petrophysical property	$\boldsymbol{m}$
Noise realization	$\boldsymbol{n}$
Noise term	$\boldsymbol{N_n}$
Prior distribution	p
Posterior distribution	P
Euclidian distance	R
Numerical simulator	$\boldsymbol{S}$
Slowness of a P-wave propagating in the horizontal direction	$s_{P,hor}$
Slowness of a P-wave propagating in the vertical direction	$s_{P,vert}$
Slowness of a horizontally polarized S-wave propagating in the horizontal direction	$s_{SH,hor}$
Slowness of a horizontally polarized S-wave propagating in the vertical direction	$s_{SH,vert}$
Slowness of a vertically polarized S-wave propagating in the horizontal direction	$s_{SV,hor}$
Slowness of a vertically polarized S-wave propagating in the vertical direction	$s_{SV,vert}$
Water saturation	S_w

Water saturation in sandstone lamina	$S_{w,n\text{-}sh,t}$
Total layer water saturation	$S_{w,T,t}$
P-wave velocity	V_p
P- to S-wave velocity ratio	V_p / V_s
S-wave velocity	V_s
Shape parameter	ϵ
Simulated bulk density log	ρ_α
Bulk density	ρ_t
Radial basis function	ϕ
Porosity of sandstone lamina	φ_m
Porosity of shale laminae	φ_{sh}
Total layer porosity	φ_T

List of acronyms

One-dimensional	1D
Three-dimensional	3D
Acoustic impedance	AI
Central processing unit	CPU
Delta-time (transit time) compressional	DTC
Delta-time (transit time) shear	DTS
Effective medium model	EMM
Logging while drilling	LWD
Markov chain Monte Carlo	MCMC
Measured depth	MD
Primary (compressional) wave	P-
Radial basis function	RBF
Bulk density (ρ_b)	RHOB
Root mean square error	RMSE
Rock physics model	RPM
Tri-axial induction resistivity tool	R_t scanner
Random-walk Markov chain Monte Carlo	RWMCMC
Shear wave	S-
Vertical transverse isotropy	VTI

References

Brie, A., Pampuri, F., Marsala, A. and Meazza, O., Shear sonic interpretation in gas-bearing sands: Presented at SPE Annual Technical Conference and Exhibition, Society of Petroleum Engineers.

Deng, T., Ambía, J. and Torres-Verdín, C., Fast Bayesian Inversion Method for the Generalized Petrophysical and Compositional Interpretation of Multiple Well Logs with Uncertainty Quantification: Presented at SPWLA 60th Annual Logging Symposium, Society of Petrophysicists and Well-Log Analysts.

Fasshauer, G. E., 2007 Meshfree approximation methods with MATLAB. World Scientific.

Gallardo, L. A. and Meju, M. A., 2004, Joint two-dimensional DC resistivity and seismic travel time inversion with cross-gradients constraints, Journal of Geophysical Research: Solid Earth, **109**(B3).

Goodyear, G., Sood, A., Andrews, M., Solomon, C. J., Luycx, M. and Torres-Verdín, C., What's New in Borehole Nuclear Modeling?(A Lot!): Presented at SPWLA 59th Annual Logging Symposium, Society of Petrophysicists and Well-Log Analysts.

Grana, D., 2013, Bayesian inversion methods for seismic reservoir characterization and time-lapse studies, Stanford University.

Grana, D. and Della Rossa, E., 2010, Probabilistic petrophysical-properties estimation integrating statistical rock physics with seismic inversion, Geophysics, **75**(3), pp. O21-O37.

Haas, A. and Dubrule, O., 1994, Geostatistical inversion-a sequential method of stochastic reservoir modelling constrained by seismic data, First break, **12**(11).

Hsu, K. and Chang, S.-K., 1987, Multiple-shot processing of array sonic waveforms, Geophysics, **52**(10), pp. 1376-1390.

Huang, S., Matuszyk, P. J. and Torres-Verdín, C., 2015, Spatial sensitivity functions for rapid numerical simulation of borehole sonic measurements in vertical wells, Geophysics, **80**(5), pp. D459-D480.

Ijasan, O., Torres-Verdín, C. and Preeg, W. E., 2013, Inversion-based petrophysical interpretation of logging-while-drilling nuclear and resistivity measurements, Geophysics, **78**(6), pp. D473-D489.

Maalouf, E. and Torres-Verdín, C., 2018a, Interpretation of borehole sonic measurements acquired in vertical transversely isotropic formations penetrated by vertical wells, Geophysics, **83**(6), pp. D187-D202.

Maalouf, E. and Torres-Verdín, C., 2018b, Inversion-based method to mitigate noise in borehole sonic logs, Geophysics, **83**(2), pp. D61-D71.

Mavko, G., Mukerji, T. and Dvorkin, J., 2020 The rock physics handbook. Cambridge university press.

Mendoza, A., Torres-Verdín, C. and Preeg, B., 2010, Linear iterative refinement method for the rapid simulation of borehole nuclear measurements: Part I—Vertical wells, Geophysics, **75**(1), pp. E9-E29.

Moyen, R., Bornard, R., Crozat, T., Doyen, P., Escobar, I., Williamson, P., Cherrett, A. and Thore, P., Bayesian stochastic inversion of seismic data in a stratigraphic grid: Presented at EAGE Conference on Petroleum Geostatistics, European Association of Geoscientists & Engineers, cp-32-00014.

Peyret, A., Torres-Verdin, C. and Xu, Y., Assessment of shoulder-bed, invasion, and lamination effects on borehole sonic logs: A numerical sensitivity study: Presented at SPWLA 47th Annual Logging Symposium, Society of Petrophysicists and Well-Log Analysts.

Quirein, J., Kimminau, S., La Vigne, J., Singer, J. and Wendel, F., A coherent framework for developing and applying multiple formation evaluation models: Presented at SPWLA 27th Annual Logging Symposium, Society of Petrophysicists and Well-Log Analysts.

Sinha, B. K., 1997, Sensitivity and inversion of borehole flexural dispersions for formation parameters, Geophysical Journal International, **128**(1), pp. 84-96.

Sinha, B. K., Vissapragada, B., Renlie, L. and Tysse, S., 2006, Radial profiling of the three formation shear moduli and its application to well completions, Geophysics, **71**(6), pp. E65-E77.

Skelt, C., 2004, Fluid substitution in laminated sands, The Leading Edge, **23**(5), pp. 485-493.

Tang, X.-M., Cheng, C. H. A. and Cheng, A., 2004 Quantitative borehole acoustic methods. Elsevier.

Tarantola, A. (1987) 'Inversion of travel times and seismic waveforms', *Seismic tomography*: Springer, pp. 135-157.

Tarantola, A., 2005 Inverse problem theory and methods for model parameter estimation. SIAM.

Tiab, D. and Donaldson, E. C., 2015 Petrophysics: theory and practice of measuring reservoir rock and fluid transport properties. Gulf professional publishing.

Yang, J., Sinha, B. K. and Habashy, T. M., A parameterized-model-based radial profiling for formation shear slowness in cased boreholes: Presented at SEG Technical Program Expanded Abstracts 2011, Society of Exploration Geophysicists, 449-453.

Yang, Q. and Torres-Verdín, C., 2015, Joint interpretation and uncertainty analysis of petrophysical properties in unconventional shale reservoirs, Interpretation, **3**(1), pp. SA33-SA49.

Zhang, T., Tang, X. and Patterson, D., Evaluation of laminated thin beds in formations using high-resolution acoustic slowness logs: Presented at SPWLA 41st Annual Logging Symposium, Society of Petrophysicists and Well-Log Analysts.